ChemComm

Accepted Manuscript

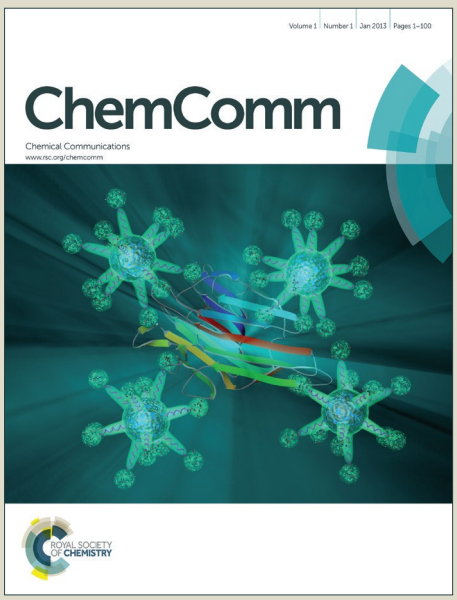

ROYAL SOCIETY OF CHEMISTRY

www.rsc.org/chemcomm

Journal Name

RSCPublishing

COMMUNICATION

Cite this: DOI: 10.1039/xoxxoooooox

Ternary NiFeMn Layered Double Hydroxides as High-efficient Oxygen Evolution Catalysts

Received ooth January 2012,
Accepted ooth January 2012

DOI: 10.1039/xoxxoooooox

www.rsc.org/

Zhiyi Lu[†a], Li Qian[†a], Yang Tian[a], Yaping Li[a], Xiaoming Sun*[a] and Xue Duan[a]

Layered double hydroxides (LDHs) are a family of layer materials with heightened attention. Herein a ternary NiFeMn-LDH is investigated with superior oxygen evolution activity, which is attributed to the Mn^{4+} doping in the intralayer, which modifies the electronic structure and improves the conductivity of the electrocatalyst.

Layered double hydroxides (LDHs), also known as anionic or hydrotalcite-like clays, are composed of layers of divalent and trivalent metal cations coordinated to hydroxide anions, with guest anions (typically CO_3^{2-}) intercalated between the layers.[1-4] Because of the unique physical and chemical properties (e.g. tunable metal species and ratio, and interlayer spacing), LDHs have been widely investigated as catalysts[5, 6], drug delivery hosts[7], flame retardants[8], and biomaterials[9]. Recent studies demonstrate that LDHs materials containing electrochemically active metal elements show attractive performances in supercapacitors[10, 11] and electrochemical catalysis[12, 13]. As a typical example, NiFe-LDHs[14-18] with conductive matrices (e.g. carbon nanotubes[19] and graphene[20]) have been widely investigated with superb activities than either of the parent metal catalyst[21, 22], and comparable to the best noble catalysts (e.g. IrO_2 and RuO_2[23]) for oxygen evolution reaction (OER), which is a key component for a number of energy storage and conversion processes[24-27]. However, current attentions are mostly concentrated on binary LDHs[28-30], while ternary LDHs which incorporate an additional metal species may offer even higher OER activities and are rarely studied so far[31].

In this work, the OER activity of ternary NiFeMn-LDHs were systematically investigated. By incorporating a certain amount of Mn into the LDH laminate, the one-pot synthesized ternary NiFeMn-LDHs with layered structure (Figure 1A) demonstrated an advanced OER performance, affording a low overpotential of ~289 mV at the current density of 20 mA cm^{-2}, small Tafel slope (~47 mV dec^{-1}), and stable operation for over 15 h, much superior to the NiFe-LDH and commercial Ir/C catalysts. This enhanced OER activity was attributed to the Mn^{4+} doping, which narrowed the bandgap and thereby improves the electric conductivity of the active material, as manifested by detailed electrochemical and DFT simulation. This study provided a convincing demonstration of ternary LDHs as cheap OER alternatives, which may also hold great potential in a variety of electrolysis systems.

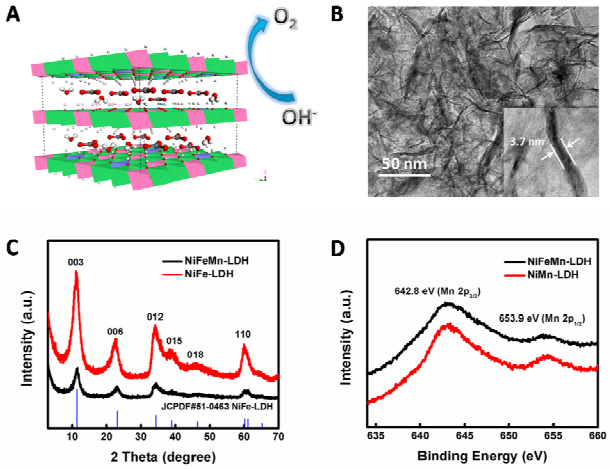

Figure 1. (A), Structural scheme of trinay NiFeMn-LDH; (B), typical TEM image of NiFeMn-LDH, the inset is the magnified image, demonstrating the thin thickness of the LDH nanoplate; (C), standard XRD pattern of NiFe-LDH and the measured XRD patterns of the as-synthesized NiFe-LDH and NiFeMn-LDH; (D), XPS results of Mn 2p in NiMn-LDH and NiFeMn-LDH, indicating that the 4+ oxidation state of Mn in both LDHs.

A simple coprecipitation method was employed to synthesize ternary NiFeMn LDHs at room temperature. An homogeneously aqueous solution containing Ni, Fe and Mn nitrates was firstly prepared with continuous bubbling of O_2, and then a certain amount of aqueous solution containing NaOH and Na_2CO_3 was added dropwisely to generate the LDHs nuclei (see Supporting Information for details). After aging for 12 h, the NiFeMn-LDHs were formed as earthy yellow precipitates. The size and morphology of the product were characterized by transmission electron microscopy (TEM), as shown in Figure 1B, which demonstrated a flower-like structure

assembled by the ternary LDHs nanoplates. High-resolution TEM image (inset of Figure 1B) revealed the average size and thickness of ~50 nm and ~3.7 nm, respectively, and the thickness corresponded to five edge-sharing octahedral MO_6 layers[1, 6, 14, 32]. The thin thickness of the nanoplate was further confirmed by the atomic force microscopy (AFM) image (Figure S1).

The X-ray diffraction (XRD) pattern was also examined to demonstrate the crystal structure of the LDHs. As shown in Figure 1C, XRD data of the NiFeMn-LDH (black line) showed a series of Bragg reflections in good agreement with the well-known NiFe-LDH (red line, JCPDF: 51-0463), indicating the Mn doping did not cause any structure deformation. The layered structure of NiMn-LDH was also demonstrated by XRD (Figure S2) The atomic ratios of transition metals in the as-synthesized samples were determined by inductively coupled plasma atomic emission spectroscopy (ICPAES, Table S1), which revealed the Ni/Fe/Mn ratios close to the ratios in the starting materials. X-ray photoelectron spectroscopy (XPS, Figure 1D and S3) demonstrated the $2p_{3/2}$ binding energies of 855.9, 713.1 and 642.8 eV for Ni, Fe and Mn, indicating oxidation states of +2, +3 and +4, respectively.[19, 33, 34] The valence states of the transition metals were similar to those in NiFe-LDH and NiMn-LDH.

The electrocatalytic OER activity of NiFeMn-LDH was investigated in alkaline solutions (1 M KOH) in a standard three-electrode system. For comparison purposes, binary NiFe-LDH, NiMn-LDH, and a commercial 20 wt% Ir/C catalyst were tested under the same condition. The catalysts were uniformly casted onto a macroporous carbon fiber paper substrate with a mass-loading of ~0.2 mg cm^{-2}, and the IR-corrected OER polarization curves were recorded at a slow scan rate of 1 mV s^{-1} to minimize capacitive current after tens of cyclic voltammetric scans to reach a relatively stable state. Figure 2A manifested that the NiFeMn-LDH catalyst afforded the earliest onset potential (~1.43 V versus reversible hydrogen electrode, RHE) and the fastest OER current increase beyond the onset potential among all the samples measured. Tafel plots derived from polarization curves (Figure 2B) revealed a small Tafel slope (~47 mV dec^{-1}) of NiFeMn-LDH, which outperformed those of binary NiFe-LDH (~65 mV dec^{-1}) and NiMn-LDH (~70 mV dec^{-1}), and the commercial Ir/C catalyst (~78 mV dec^{-1}), confirming the highest OER activity. Moreover, to reach a certain current density (e.g. 20 mA cm^{-2}), the as-prepared NiFeMn-LDH only required an overpotential (η) of ~289 mV, which was 112, 351, and 141 mV less than NiFe-LDH, NiMn-LDH, and Ir/C catalyst, respectively (Figure 2C). A TOF value of 0.038 s^{-1} was calculated for the NiFeMn-LDH at η of 300 mV, assuming all the metal sites were involved in the electrochemical reaction (the calculation details can be seen in SI). This value was much higher than those of the reference materials, as list in Table S2.

It should be noted that the OER activity of the ternary NiFeMn-LDH after composition optimization was better or comparable than the previous reported LDHs[12, 19, 35] and high-performance OER catalysts (e.g. peroveskites[36, 37], phosphates[38, 39] and mixed metal oxides[40-42]), as summerized in Table S3. In addition, the effect of transition metal ratios on the OER activity was investigated by varying the ratio from 3:1:0.25 to 3:1:2. The results demonstrated that the OER activity of NiFeMn-LDH was highly dependent on the doping amount of Mn and the optimized transitional metal ratio of Ni, Fe and Mn was 3:1:0.5, as shown in Figure 2D.

Besides the high OER activity, the ternary LDH catalyst exhibited prominent durability in alkaline solutions, as revealed by plotting the current density/potential vs time curves (Figure 3A). By applying a constant overpotential, a stable corresponding current density (~20 mA cm^{-2}) was observed for over 15 hours. In addition, when biased galvanostatically at 10 mA cm^{-2}, the NiFeMn-LDH catalyst showed a nearly constant operating potential of ~1.54 V (corresponding to η of 310 mV).

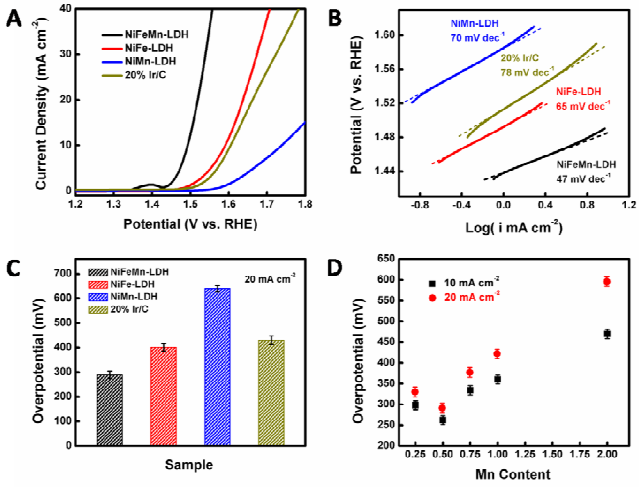

Figure 2. (A), polarization curves of three LDHs catalysts (NiFeMn-LDH, NiFe-LDH and NiMn-LDH) and commercial Ir/C catalyst, the NiFeMn-LDH shows the lowest onset potential and fastest current density increase; (B), the corresponding Tafel plots of the four catalysts; (C), the required overpotentials comparison of four catalysts at the current density of 20 mA cm^{-2}; (D), overpotentials comparisons of the Mn content in the ternary LDHs under different current densities, the optimized transition metal ratio is 3:1:0.5 for Ni, Fe and Mn. The error bars are obtained by at least 5 times measurement.

Detailed electrochemical and structural analysis on the ternary NiFeMn-LDH may shed light on tracing the source for the improved OER activity. Generally the electrochemical surface area (ESA) is believed to be responsible for the high electrocatalytic activity.[43, 44] Because the doping amount of Mn was relatively small and LDHs possessed similar layered structure, the electrochemical double layer capacitances (C_{dl}) was a reasonable parameter to represent their ESAs. Figure 3B and S4 demonstrated that, by measuring the double layer current densities at the non-Faradic region (0-0.05 V vs. SCE), the NiFeMn-LDH possessed a 3 times higher C_{dl} than that of NiFe-LDH. The much higher C_{dl} of the ternary LDH contributed to the higher OER activity and was attributed to the higher electric conductivity as the NiFeMn-LDH and NiFe-LDH showed similar size and morphology (Figure S5). We have also tested the OER performance of NiFe-LDH electrode with comparable C_{dl} to the NiFeMn-LDH by simply increasing the loading of the active material, and the results demonstrated that the NiFeMn-LDH was still better than NiFe-LDH (Figure S6), indicating the high intrinsic activity of NiFeMn-LDH.

Since the NiFeMn-LDH showed a smaller Tafel slope which was usually influenced by electron and mass transport[12], the scan rate dependence of the activity of NiFeMn-LDH was performed to exclude the possible effect of mass transport process. Negligible change in OER activity was found on the NiFeMn-LDH by increasing the scan rate from 1 to 10 mV s^{-1} (Figure 3C), suggesting that mass transport was sufficiently rapid. Thus, the lower Tafel slope of NiFeMn-LDH was likely due to faster electron transport in the active material.

The above electrochemical analysis demonstrated that Mn^{4+} doping into the laminate of NiFe-LDH could accelerate the electron transport process. To deeply understand the doping effect, the

electronic structures of NiFe-LDH and NiFeMn-LDH were calculated by a density function theory plus U (DFT+U) method. As shown in the total densities of states (TDOSs) and the projected densities of states (PDOSs) curves (Figure 4A), the bandgap between the valence and conduction bands of NiFe-LDH was about 2.1 eV, while a narrower bandgap was observed after doping with the Mn^{4+} ion, indicating a more conductive electronic structure[45]. The reduced band gap of NiFeMn-LDH was also confirmed by the UV-vis diffuse spectrum (Figure S7). In addition, the sheet resistance of NiFe-LDH disk shape pellet was measured to be 2.2×10^3 Ω sq^{-1}, while the sheet resistance of NiFeMn-LDH pellet was 1.6×10^3 Ω sq^{-1}, directly proving the higher conductivity of NiFeMn-LDH. Moreover, it is reported recently that Ni-based hydroxides with Fe or Mn doping could adjust the adsorption energies difference between *O and *OH, achieving better OER activities.[29]

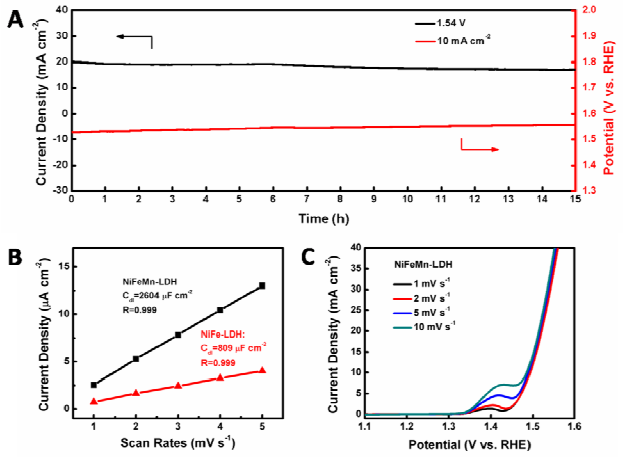

Figure 3. (A), The potentiostatic and galvanostatic stability testing under a certain potential or current density, the corresponding current density or potential can be stable for over 15 h, demonstrating the high stability. (B), the C_{dl} calculations of NiFeMn-LDH and NiFe-LDH; (C), polarization curves of the NiFeMn-LDH measured under various scan rates.

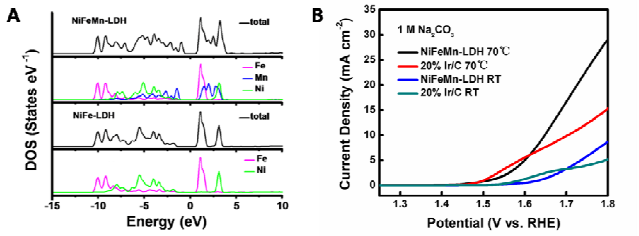

Figure 4. (A), Total DOS (TDOS) and partial DOS (TDOS) curves of NiFeMn-LDH and NiFe-LDH, the narrower bandgap of NiFeMn-LDH indicates a more conductive structure; (B); polarization curves of ternary LDH nad commercial Ir/C catalysts in 1 M Na_2CO_3 electrolyte under room temperature and 70 ℃, the ternary LDH shows a higher activity, demonstrating the potential application as anode material for Na_2CO_3 electrolysis.

The advanced electrochemical and electronic metrics endowed the NiFeMn-LDH with other electro-catalysis applications. Firstly the NiFeMn-LDH was investigated as the anode material for electrolysis of Na_2CO_3[46], which was an advanced electrochemical process for purification of alumina. Electrochemical result (Figure 4B) demonstrated that NiFeMn-LDH showed an earlier onset potential and faster current density increase than the Ir/C catalyst under room temperature and 70℃, indicating a superior catalytic performance. In addition, the NiFeMn-LDH also exhibited reasonable performance for oxygen reduction reaction (ORR), as shown in Figure S8. Therefore, this ternary LDH is a multi-functional electrocatalyst for a variety of energy conversion processes, including regenerative fuel cells and metal-air batteries.

In summary, a ternary LDH containing Ni, Fe and Mn fabricated by one-pot synthesis was reported for the first time as an efficient electrocatalyst for water oxidation. The NiFeMn-LDH showed an excellent OER activity, superior to the NiFe-LDH and commercial Ir/C catalyst in terms of the onset potential, Tafel slopes and OER current densities at certain overpotentials. This high OER activity of the NiFeMn-LDH was mostly attributed to the Mn^{4+} doping into the laminate of the layered structure, which affected the electronic structure and thereby improved the electric conductivity, as revealed by detailed electrochemical and DFT investigations. Moreover, a prominent OER stability was observed on the NiFeMn-LDH. This study not only suggest the promise of ternary LDH as an efficient, robust and cost-effective water oxidation electrocatalyst, but also open up an opportunity on the rational design of advanced electrocatalysts towards global scale clean energy production.

This work was supported by NSFC, 973 Program (2011CBA00503, 2012CB93280), the 863 Program (2012AA03A609), the Program for Changjiang Scholars and Innovative Research Team in University.

Notes and references

[a] *State Key Laboratory of Chemical Resource Engineering, College of Energy, Beijing University of Chemical Technology, Beijing 100029, China*

Tel.: +86-10-64448751. Fax: +86-10-64425385.

E-mail: sunxm@mail.buct.edu.cn

† Contributed equally to this work

Electronic Supplementary Information (ESI) available: [experimental section, AFM image, XPS patterns, C_{dl} measurements, XRD pattern of NiMn-LDH, TEM image of NiFe-LDH, UV-vis diffuse reflectance spectra and ORR performance]. See DOI: 10.1039/c000000x/

1. Q. Wang and D. O'Hare, *Chem. Rev.*, 2012, **112**, 4124-4155.
2. D. G. Evans and R. C. T. Slade, in *Layered Double Hydroxides*, eds. X. Duan and D. G. Evans, Springer-Verlag Berlin, Berlin, 2006, vol. 119, pp. 1-87.
3. X. Guo, F. Zhang, D. G. Evans and X. Duan, *Chem. Commun.*, 2010, **46**, 5197-5210.
4. D. G. Evans and X. Duan, *Chem. Commun.*, 2006, **37**, 485-496.
5. B. Sels, D. De Vos, M. Buntinx, F. Pierard, A. Kirsch-De Mesmaeker and P. Jacobs, *Nature*, 1999, **400**, 855-857.
6. G. L. Fan, F. Li, D. G. Evans and X. Duan, *Chem. Soc. Rev.*, 2014, **43**, 7040-7066.
7. A. Alcantara, P. Aranda, M. Darder and E. Ruiz-Hitzky, *J. Mater. Chem.*, 2010, **20**, 9495-9504.
8. C. Manzi-Nshuti, J. M. Hossenlopp and C. A. Wilkie, *Polym. Degrad. Stab.*, 2009, **94**, 782-788.
9. H. B. Yao, Z. H. Tan, H. Y. Fang and S. H. Yu, *Angew. Chem. Int. Ed.*, 2010, **49**, 10127-10131.

10. J. Zhao, J. Chen, S. Xu, M. Shao, Q. Zhang, F. Wei, J. Ma, M. Wei, D. G. Evans and X. Duan, *Adv. Funct. Mater.*, 2014, **24**, 2938-2946.
11. Z. Lu, X. Wu, M. Jiang, J. Wang, J. Liu, X. Lei and X. Sun, *Sci. China. Mater.*, 2014, **57**, 59-69.
12. F. Song and X. Hu, *J. Am. Chem. Soc.*, 2014, **136**, 16481-16484.
13. W. Huang, H. Zhong, D. Li, P. Tang and Y. Feng, *Electrochim. Acta*, 2015, **173**, 575-580.
14. F. Song and X. Hu, *Nat. Commun.*, 2014, **5**, 4477-4486.
15. M. A. Oliver-Tolentino, J. Vázquez-Samperio, A. Manzo-Robledo, R. d. G. González-Huerta, J. L. Flores-Moreno, D. Ramírez-Rosales and A. Guzmán-Vargas, *J. Phys. Chem. C*, 2014, **118**, 22432-22438.
16. J. Luo, J.-H. Im, M. T. Mayer, M. Schreier, M. K. Nazeeruddin, N.-G. Park, S. D. Tilley, H. J. Fan and M. Graetzel, *Science*, 2014, **345**, 1593-1596.
17. X. Lu and C. Zhao, *Nat. Commun.*, 2015, **6**, 6616-6623.
18. D. H. Youn, Y. Bin Park, J. Y. Kim, G. Magesh, Y. J. Jang and J. S. Lee, *J. Power Sources*, 2015, **294**, 437-443.
19. M. Gong, Y. Li, H. Wang, Y. Liang, J. Z. Wu, J. Zhou, J. Wang, T. Regier, F. Wei and H. Dai, *J. Am. Chem. Soc.*, 2013, **135**, 8452-8455.
20. X. Long, J. Li, S. Xiao, K. Yan, Z. Wang, H. Chen and S. Yang, *Angew. Chem. Int. Ed.*, 2014, **126**, 7714-7718.
21. L. Trotochaud, J. K. Ranney, K. N. Williams and S. W. Boettcher, *J. Am. Chem. Soc.*, 2012, **134**, 17253-17261.
22. J. Moir, N. Soheilnia, P. O'Brien, A. Jelle, C. M. Grozea, D. Faulkner, M. G. Helander and G. A. Ozin, *ACS nano*, 2013, **7**, 4261-4274.
23. Y. Lee, J. Suntivich, K. J. May, E. E. Perry and Y. Shao-Horn, *J. Phys. Chem. Lett.*, 2012, **3**, 399-404.
24. Y. Li, M. Gong, Y. Liang, J. Feng, J.-E. Kim, H. Wang, G. Hong, B. Zhang and H. Dai, *Nat. Commun.*, 2013, **4**, 1805-1811.
25. C. Li, X. Han, F. Cheng, Y. Hu, C. Chen and J. Chen, *Nat. Commun.*, 2015, **6**, 7345-7353.
26. H. Wang, H.-W. Lee, Y. Deng, Z. Lu, P.-C. Hsu, Y. Liu, D. Lin and Y. Cui, *Nat. Commun.*, 2015, **6**, 7261-7269.
27. W. He, C. Jiang, J. Wang and L. Lu, *Angew. Chem. Int. Ed.*, 2014, **53**, 9503-9507.
28. J. Nai, H. Yin, T. You, L. Zheng, J. Zhang, P. Wang, Z. Jin, Y. Tian, J. Liu and Z. Tang, *Adv. Energy. Mater.*, 2015, **10.1002/aenm.201401880**.
29. O. Diaz-Morales, I. Ledezma-Yanez, M. T. Koper and F. Calle-Vallejo, *ACS Catal.*, 2015, 5380-5387.
30. S. Chen, J. Duan, P. Bian, Y. Tang, R. Zheng and S. Z. Qiao, *Adv. Energy Mater.*, 2015, **10.1002/aenm.201500936**.
31. L. Qian, Z. Lu, T. Xu, X. Wu, Y. Tian, Y. Li, Z. Huo, X. Sun and X. Duan, *Adv. Energy Mater.*, 2015, **10.1002/aenm.201500245**.
32. G. Abellán, E. Coronado, C. Martí-Gastaldo, E. Pinilla-Cienfuegos and A. Ribera, *J. Mater. Chem.*, 2010, **20**, 7451-7455.
33. Z. Lu, W. Xu, W. Zhu, Q. Yang, X. Lei, J. Liu, Y. Li, X. Sun and X. Duan, *Chem. Commun.*, 2014, **50**, 6479-6482.
34. J. Zhao, J. Chen, S. Xu, M. Shao, D. Yan, M. Wei, D. G. Evans and X. Duan, *J. Mater. Chem. A*, 2013, **1**, 8836-8843.
35. Y. Li, L. Zhang, X. Xiang, D. Yan and F. Li, *J. Mater. Chem. A*, 2014, **2**, 13250-13258.
36. J. Suntivich, K. J. May, H. A. Gasteiger, J. B. Goodenough and Y. Shao-Horn, *Science*, 2011, **334**, 1383-1385.
37. A. Grimaud, K. J. May, C. E. Carlton, Y.-L. Lee, M. Risch, W. T. Hong, J. Zhou and Y. Shao-Horn, *Nat. Commun.*, 2013, **4**, 2439-2446.
38. M. W. Kanan and D. G. Nocera, *Science*, 2008, **321**, 1072-1075.
39. H. S. Ahn and T. D. Tilley, *Adv. Funct. Mater.*, 2013, **23**, 227-233.
40. J. B. Gerken, S. E. Shaner, R. C. Massé, N. J. Porubsky and S. S. Stahl, *Energy Environ. Sci.*, 2014, **7**, 2376-2382.
41. R. D. Smith, M. S. Prévot, R. D. Fagan, Z. Zhang, P. A. Sedach, M. K. J. Siu, S. Trudel and C. P. Berlinguette, *Science*, 2013, **340**, 60-63.
42. Y. Yang, H. Fei, G. Ruan, C. Xiang and J. M. Tour, *ACS nano*, 2014, **8**, 9518-9523.
43. D. Merki, H. Vrubel, L. Rovelli, S. Fierro and X. Hu, *Chem. Sci.*, 2012, **3**, 2515-2525.
44. J. Kibsgaard, Z. Chen, B. N. Reinecke and T. F. Jaramillo, *Nat. Mater.*, 2012, **11**, 963-969.
45. Y. Wang, T. Zhou, K. Jiang, P. Da, Z. Peng, J. Tang, B. Kong, W. B. Cai, Z. Yang and G. Zheng, *Adv. Energy Mater.*, 2014, **10.1002/aenm.201400696**.
46. Z. Yu, Y. Chen, Y. Niu, Y. Tang, P. Wan, Z. Lv and X. J. Yang, *Angew. Chem. Int. Ed.*, 2011, **123**, 11923-11927.